Translational Symmetries in the Linear-Chain Semiconductors $K_4[Pt_2(P_2O_5H_2)_4X]\cdot nH_2O$ (X = Cl, Br, I)

Leslie G. Butler,*[1a] Miriam Heinrichs Zietlow,[1b] Chi-Ming Che,[1c] William P. Schaefer,*[1b] S. Sridhar,[1d] Paula J. Grunthaner,[1e] Basil I. Swanson,*[1f] Robin J. H. Clark,[1g] and Harry B. Gray*[1b]

Contribution No. 7609 from the Arthur Amos Noyes Laboratory, California Institute of Technology, Pasadena, California 91125, Department of Chemistry, Louisiana State University, Baton Rouge, Louisiana 70803, and Isotopic and Structural Chemistry Group (INC-4), Los Alamos National Laboratory, Los Alamos, New Mexico 87545. *Received June 15, 1987*

Abstract: The solid-state structures of the linear-chain semiconductors $K_4[Pt_2(P_2O_5H_2)_4X]\cdot nH_2O$ (X = Cl, Br, I), abbreviated Pt_2Cl, Pt_2Br, and Pt_2I, have been studied. The X-ray crystal structures of Pt_2Cl at 300 and 22 K and of Pt_2Br at 19 K are reported. These structures show that Pt_2Cl is a composite of alternating units of Pt_2 and Pt_2Cl_2 with $(AABCCB)_n$ translational symmetry. The X-ray structure of Pt_2Br, on the other hand, shows equivalent Pt-Pt bonds and two slightly different Pt-Br bonds. Raman data confirm the composite Pt_2/Pt_2Cl_2 structure for Pt_2Cl and indicate that the Pt_2Br species is comprised of dimeric units with nearly equal Pt-Pt bonds. The Pt_2Br structure is viewed as involving a slight distortion from idealized $(AAB)_n$ toward $(AABCCB)_n$ translational symmetry. Structural studies of Pt_2I were attempted; however, all crystals were twinned. Magnetic susceptibility, microwave conductivity, ESCA, and reflectance spectroscopy measurements are reported for Pt_2Br; the material is a semiconductor, with $\sigma = 10^{-3}\ \Omega^{-1}\ cm^{-1}$ at 300 K, a bandgap of 0.08 eV, and a bandwidth greater than 0.05 eV.

Materials having anisotropic electrical conductivity, whether built from aromatic organic molecules or transition-metal complexes, have been the subject of much contemporary research.[2-8] The electronic properties of a linear chain are determined by the extent of interaction between neighboring atoms along the chain and by the translational symmetry of the linear chain. While the importance of the overlap between atomic orbitals of neighboring atoms in the linear chain has been discussed,[9-11] little attention has been directed to the desired characteristics of the translational symmetry[12] required for optimization of a property such as electrical conductivity. (Indeed, the mechanisms of electrical transport in these materials are unknown. To date, the variety of translational symmetry types in linear chains has been limited. $K_2Pt(CN)_4Br_{0.3}\cdot 3.2H_2O$ is typical of the near-perfect $(A)_n$ symmetry found in most linear-chain systems made from mononuclear transition-metal complexes.[6,13] Tetrathiafulvalenium tetracyanoquinodimethanide, TTF-TCNQ, with $(A)_n$ along each of the two segregated stacks of TTF cations and TCNQ anions, is representative of 1-dimensional organic conductors.[2,5,14] Salts of tetramethyltetraselenafulvalene, such as $[(TMTSF)_2(ReO_4)]$, also have this symmetry and are members of the first class of linear-chain compounds that have been found to undergo a transition to a superconductive phase.[15-17]

We have been concerned with the bonding in d^8-d^8 transition-metal dimers, such as $Rh_2b_4^{+2}$ (b = diisocyanopropane).[18-22] The rhodium dimer has interesting photophysical properties resulting from metal-metal interactions. For example, the lowest excited electronic state ($^3A_{2u}$; $(d\sigma)^2(d\sigma^*)^1(p\sigma)^1$) possesses a relatively strong Rh-Rh bond.[21,22] Interestingly, some of the rhodium isocyanides are 1-dimensional materials.[23] In our studies of d^8-d^8 platinum complexes, we discovered a material that contained a linear chain of $[Pt_2(P_2O_5H_2)_4]^{4-}$ units bridged by a halide ion[24-27] and having a metallic luster. The 300 K X-ray structure of Pt_2Br ($Pt_2X = K_4[Pt_2(P_2O_5H_2)_4X]$; X = Cl, Br, I) has been reported;[28] it revealed an apparent $(AAB)_n$ linear-chain system that prompted us to investigate the properties of this unusual system. Some of the possible translational geometries for the three-atom repeat unit of Pt_2X are shown in Figure 1. In the present paper, we focus on the structures of the 1-dimensional materials, the existence of temperature-dependent phase transitions, if any, and the question of which of these structural schemes is valid for the Pt_2X system.

During the course of this work, the preparation and room-

(1) (a) Louisiana State University. (b) California Institute of Technology. (c) Present address: Department of Chemistry, University of Hong Kong, Pokfulam Rd., Hong Kong. (d) Present address: Department of Physics, University of California at Los Angeles, Los Angeles, CA 90024. (e) Present address: Jet Propulsion Laboratory, Pasadena, CA 91109. (f) Los Alamos National Laboratory. (g) Present address: University College, London, WCIHOAJ, England.

(2) Williams, J. M.; Beno, M. A.; Wang, H. H.; Leung, P. C. W.; Emge, T. J.; Geiser, U.; Carlson, K. D. *Acc. Chem. Res.* **1985**, *18*, 261.
(3) Miller, J. S., Ed. *Extended Linear Chain Compounds*; Plenum: New York, 1982; Vol. 1-3.
(4) Monceau, P., Ed. *Electronic Properties of Inorganic Quasi-One-Dimensional Compounds*; D. Reidel: Boston, 1985; Vol. 1 and 2.
(5) Ibers, J. A.; Pace, L. J.; Martinsen, J.; Hoffman, B. M. *Struct. Bonding (Berlin)* **1982**, *50*, 1.
(6) Stucky, G. D.; Schultz, A. J.; Williams, J. M. *Annu. Rev. Mater. Sci.* **1977**, *7*, 301.
(7) Toombs, G. A. *Phys. Rev.* **1978**, *40*, 181.
(8) Friend, R. H.; Jerome, D. *J. Phys. C* **1979**, *12*, 1441.
(9) Whangbo, M.-H.; Hoffmann, R. *J. Am. Chem. Soc.* **1978**, *100*, 6093.
(10) Hoffmann, R.; Christian, M.; Gray, H. B. *J. Am. Chem. Soc.* **1984**, *106*, 2001.
(11) Whangbo, M.-H. *Acc. Chem. Res.* **1983**, *16*, 95.
(12) Whangbo, M.-H. Canadell, E. *Inorg. Chem.* **1986**, *25*, 1762.
(13) Peters, C.; Eagen, C. F. *Inorg. Chem.* **1976**, *15*, 782.
(14) Schultz, A. J.; Stucky, G. D.; Blessing, R. H.; Coppens, P. *J. Am. Chem. Soc.* **1976**, *98*, 3194.
(15) Jerome, D.; Mazaud, A.; Ribault, M.; Bechgaard, K. *J. Phys., Lett.* **1980**, *41*, L195.
(16) Bechgaard, K.; Carneiro, K.; Olsen, M.; Rasmussen, F. B.; Jacobsen, C. S. *Phys. Rev. Lett.* **1981**, *46*, 852.
(17) Bechgaard, K.; Rasmussen, F. B.; Olsen, M.; Rindorf, G.; Jacobsen, C. S.; Pedersen, H. J.; Scott, J. C. *J. Am. Chem. Soc.* **1981**, *103*, 2440.
(18) Mann, K. R.; Gordon, J. G., II; Gray, H. B. *J. Am. Chem. Soc.* **1975**, *97*, 3553.
(19) Balch, A. L.; Olmstead, M. M. *J. Am. Chem. Soc.* **1976**, *98*, 2354.
(20) Sigal, I. S.; Gray, H. B. *J. Am. Chem. Soc.* **1981**, *103*, 2220.
(21) Rice, S. F.; Gray, H. B. *J. Am. Chem. Soc.* **1981**, *103*, 1593.
(22) Dallinger, R. F.; Miskowski, V. M.; Gray, H. B.; Woodruff, W. H. *J. Am. Chem. Soc.* **1981**, *103*, 1595.
(23) Gordon, J. G., II; Williams, R.; Hsu, C.-H.; Cuellar, E.; Samson, S.; Mann, K.; Gray, H. B.; Hadek, V.; Somoano, R. *Ann. N.Y. Acad. Sci.* **1978**, *313*, 580.
(24) Filomena Dos Remedios Pinto, M. A.; Sadler, P. J.; Neidle, S.; Sanderson, M. R.; Subbiad, A.; Kuroda, R. *J. Chem. Soc., Chem. Commun.* **1980**, 13.
(25) Che, C.-M.; Butler, L. G.; Gray, H. B. *J. Am. Chem. Soc.* **1981**, *103*, 7796.
(26) Che, C.-M.; Butler, L. G.; Grunthaner, P. J.; Gray, H. B. *Inorg. Chem.* **1985**, *24*, 4662.
(27) Isci, H.; Mason, W. R. *Inorg. Chem.* **1985**, *24*, 1761.
(28) Che, C.-M.; Herbstein, F. H.; Schaefer, W. P.; Marsh, R. E.; Gray, H. B. *J. Am. Chem. Soc.* **1983**, *105*, 4606.

0002-7863/88/1510-1155$01.50/0 © 1988 American Chemical Society

Table I. Crystal and Intensity Data Collection Summary[a]

	Pt_2Br at 19 K	Pt_2Cl at 300 K	Pt_2Cl at 22 K
molecular formula	$K_4[Pt_2(P_2O_5H_2)_4Br]\cdot 3H_2O$	$K_4[Pt_2(P_2O_5H_2)_4Cl]\cdot 3H_2O$	$K_4[Pt_2(P_2O_5H_2)_4Cl]\cdot 3H_2O$
a, Å	13.131 (3)	13.283 (3)	13.170 (4)
c, Å	8.139 (3)	8.125 (3)	8.077 (3)
cryst dimen, mm	0.24 × 0.21 × 0.20	0.10 × 0.14 × 0.26	0.22 × 0.15 × 0.08
abs coeff, μ(Mo Kα), cm^{-1}	131.4	114.8	116.9
transmissn coeff: min, max	0.077, 0.199	0.221, 0.343	0.193, 0.407
2θ limits, deg	2.0–75.0	3.0–75.0	5.0–80.0
no. of reflcn collcd	5097	4112	3335
no. of unique reflcn	2050	2095	1428
no. of reflcn with $I > 0$	1838	1820	1333
refined param	54	63	61
R^b	0.055	0.056	0.036
GOF[c]	3.3	2.2	2.0

[a] For all three compounds, the space group is $P4/mbm$ (No. 127), with $Z = 2$. [b] $R = (\sum||F_o| - |F_c||)/\sum F_o$, based upon data with $I > 0$. [c] GOF = $[\sum w(F_o^2 - F_c^2)^2/(n-p)]^{1/2}$.

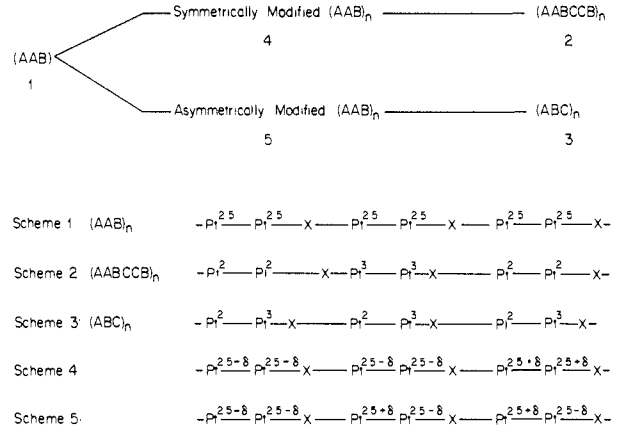

Figure 1. Translational symmetries for Pt_2X.

temperature X-ray structures of an analogous 1-dimensional system, $Ni_2(CH_3CS_2)_4I$ and $Pt_2(CH_3CS_2)_4I$, were reported.[29] Also, the 300 K structure of $K_4[Pt_2(P_2O_5H_2)_4Cl]\cdot 3H_2O$ has been independently determined and reported, together with Raman and infrared data for $K_4[Pt_2(P_2O_5H_2)_4X]\cdot nH_2O$ (X = Cl, Br, I).[30] Band-theory calculations have been done for the general Pt_2X system.[12]

Experimental Section

Preparation of $K_4[Pt_2(P_2O_5H_2)_4Cl]\cdot 3H_2O$, Pt_2Cl. The preparations of both Pt_2Cl and Pt_2Br are similar in that Pt_2 and Pt_2X_2 ($Pt_2 = K_4[Pt_2(P_2O_5H_2)_4]$ and $Pt_2X_2 = K_4[Pt_2(P_2O_5H_2)_4X_2]$; X = Cl, Br, I) are the reactants. However, an improved method for preparing the reduced parent metal dimer, $K_4[Pt_2(P_2O_5H_2)_4]\cdot 2H_2O$, was used.[26] A total of 0.08 g of $K_4[Pt_2(P_2O_5H_2)_4]$ and 0.08 g of $K_4[Pt_2(P_2O_5H_2)_4Cl_2]$ were dissolved in a minimum amount of water together with 0.4 g of KNO_3. Absolute methanol was added dropwise until a dark precipitate began to form. A few drops of water were added to clarify the solution. The solution was then cooled slowly to 5 °C and allowed to stand for 2 days. The bronze crystals were filtered and dried. (Anal. Calcd for $K_4[Pt_2(P_2O_5H_2)_4Cl]\cdot 3H_2O$; Pt, 32.19; P, 20.45; Cl, 2.93. Found: Pt, 32.4; P, 20.6; Cl, 2.82.

Preparation of $K_4[Pt_2(P_2O_5H_2)_4Br]\cdot 3H_2O$, Pt_2Br. Pt_2Br was prepared from $K_4[Pt_2(P_2O_5H_2)_4]$ by the published procedure.[28] Weissenberg photographs showed a diffraction pattern at 300 K identical with that observed in the earlier X-ray structure determination.

We note that the appearance of Pt_2Cl and Pt_2Br under transmitted light shows sample dependence, which manifests itself as subtle differences in the Raman data. This sample dependence will be discussed later.[31]

Preparation of $K_4[Pt_2(P_2O_5H_2)_4I]\cdot nH_2O$, Pt_2I. Dark, metallic crystals of Pt_2I were prepared by the published procedure.[28]

Magnetic Susceptibility. The magnetic susceptibilities of Pt_2Cl, Pt_2Br, and Pt_2I were measured at 10 kG from 1.7 to 300 K with an SHE Corp. Model 905 susceptometer with SQUID magnetic moment detection. The magnetic susceptibility depended on the particle size of the sample, with finely powdered samples having a larger paramagnetic contribution to the total susceptibility than crystalline samples. This dependence on the form of the sample has been observed in other 1-dimensional materials and is attributed to the formation of site defects.[32] The reported data for all of the complexes were obtained with crystalline samples. Correction for the susceptibility of the sample bucket was made by a spline-fit method.

ESCA. The X-ray photoelectron spectra were measured on a Hewlett-Packard 5950A ESCA spectrometer equipped with a low-energy flood gun. This spectrometer utilizes a monochromatic Mg Kα X-ray source. Samples were mounted on single-crystal silicon disks lightly coated with Vaseline. All spectra were taken at approximately 250 K and referenced to the aliphatic carbon 1s signal at 285 eV.

Raman and Far-IR Spectroscopy. Raman spectra of single crystals of Pt_2Cl and Pt_2Br were obtained with 676.4-nm excitation at several temperatures in the range 25–300 K. The crystals were mounted in a cell containing ca. 150 psi (room temperature) of He in order to minimize local heating. The cell was coupled to the cold end of an Air Products Displex closed-cycle cryostat and the temperature monitored and controlled by thermocouples. The spectra were obtained by a SPEX 1401 double monochromator with excitation from a Spectra Physics 171 Kr^+ laser.

Far-IR transmission spectra were obtained at several temperatures for Nujol mulls of the samples coupled to a highly reflective copper substrate. The copper substrate was coupled to the cold end of an Air Products He-flow cryostat and the temperature controlled in the range 4–300 K. The spectra were obtained by a Digilab FTS-20 vacuum FTIR, equipped with a He-cooled Ge bolometer, with nominal 0.5-cm^{-1} resolution. Typically, 100 scans were coadded to optimize the signal to noise.

Reflectance Spectroscopy. Diffuse reflectance spectra of Pt_2Br were determined with a Beckman 5550 spectrometer with a total reflectance attachment.

Electrical Conductivity. The small size of the Pt_2X crystals precluded standard dc conductivity measurements by the four-point probe technique. Also, we were concerned about the usual method of attaching leads to a crystal via silver paste, given the possibility for precipitation of silver halide and thus formation of high-resistance contacts at the crystal surface. Ac electrical conductivity was measured for Pt_2Br by a contactless microwave method with a 10-GHz resonant cavity.[33]

Crystal Structure Determinations. The general features of all crystal structure determinations were the same. The parameters of Pt_2Br at 19 K, Pt_2Cl at 22 K, and Pt_2Cl at 300 K were all refined in the tetragonal space group $P4/mbm$ (No. 127). A summary of the crystal and intensity collection data for all structures is given in Table I. All crystals were mounted with epoxy on glass fibers. The 300 K diffraction data were taken on a Syntex $P2_1$; low-temperature data sets were taken on a locally modified Syntex $P\bar{1}$ diffractometer.[34] Both diffractometers were equipped with graphite-monochromated Mo Kα X-radiation (λ = 0.71073 Å). Cell dimensions, given in Table I, were determined from

(29) (a) Bellitto, C.; Flamini, A.; Gastaldi, L.; Scaramuzza, L. *Inorg. Chem.* **1983**, *22*, 444. (b) Bellito, C.; Dessy, G.; Fares, V. *Inorg. Chem.* **1985**, *24*, 2815.

(30) (a) Clark, R. J. H.; Kurmoo, M. *J. Chem. Soc., Dalton Trans.* **1985**, 579. (b) Kurmoo, M.; Clark, R. J. H. *Inorg. Chem.* **1985**, *24*, 4420. (c) Clark, R. J. H.; Kurmoo, M.; Dawes, H. M.; Hursthouse, M. B. *Inorg. Chem.* **1986**, *25*, 409.

(31) Swanson, B. I.; Conradson, S. D.; Stroud, M. A.; Zietlow, M. H.; Gray, H. B., to be submitted for publication.

(32) Hatfield, W. E.; ter Haar, L. W. *Annu. Rev. Mater. Sci.* **1982**, *12*, 177.

(33) Buranov, J. I.; Schegolev, I. F. *Probl. Tekh. Esp.* **1971**, *2*, 171.

(34) Samson, S.; Goldish, E.; Dick, J. *J. Appl. Crystallogr.* **1980**, *13*, 425.

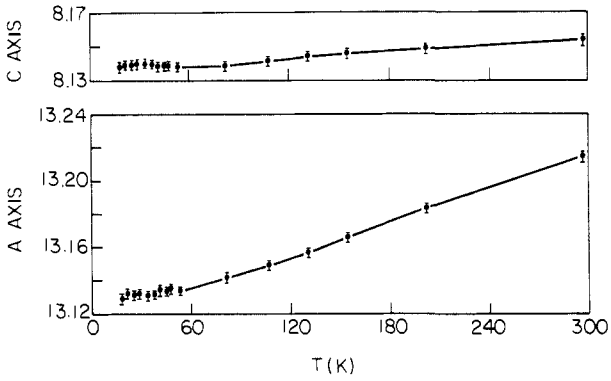

Figure 2. Dimensions of the tetragonal unit cell of Pt_2Br.

Table II. Parameters for Pt_2Br at 19 K

atom	10^4x	10^4y	10^4z	10^4U_{eq}[a]	POP[b]
Pt	0	0	3291 (0.4)	55 (0.4)	4.0
Br	0	0	122 (5)	1.15 (3)[c]	2.0
K1	2739 (3)	7739	0	218 (5)	4.0
K2	3898 (3)	8898	5000	178 (4)	4.0
P	1201 (1)	1306 (1)	3204 (1)	125 (3)	16.0
O1	2172 (3)	1026 (3)	2167 (5)	179 (10)	16.0
O2	845 (3)	2341 (3)	2636 (5)	195 (12)	16.0
O3	1708 (4)	1470 (4)	5000	266 (19)	8.0
W1	1024 (13)	6024	5215 (32)	1.8 (3)[c]	3.0
W2	551 (15)	5551	2701 (20)	1.7 (3)[c]	3.0

[a] $U_{eq} = {}^1/_3(U_{11} + U_{22} + U_{33})$. [b] Atoms per unit cell. [c] B_{iso}.

the setting angles of 15 reflections with $25° < 2\theta < 30°$. The temperatures reported for the Syntex P$\bar{1}$ data sets have error limits of ±1 K.

Data were collected by θ–2θ scans at 2°/min (from $2\theta(K\alpha_1) - 1°$ to $2\theta(K\alpha_2) + 1°$). The three check reflections collected after every 97 reflections showed a slight decrease in intensity in all crystals (~3%). Variances, $\sigma^2(I)$, were assigned on the basis of counting statistics plus an additional term, $(0.024I)^2$, to account for fluctuations proportional to the diffracted intensity. Intensities were corrected for Lorentz and polarization effects and crystal decay. With the crystal dimensions and the linear absorption coefficient, the data were corrected for absorption by Gaussian integrations over an 8 × 8 × 8 grid. All structures were refined by full-matrix least-squares techniques, minimizing $\sum w(F_o^2 - F_c^2)^2$, where $w = 1/\sigma^2(F_o^2)$. For all three structures, final difference maps were somewhat noisy, particularly in the plane containing the potassium ions and the water molecules. Alternative descriptions of the water would be consistent with the data. Residual peaks and holes (up to ±2.9 e Å^{-3}) near the potassium ion positions suggest that some changes could be made in their description, but we did not develop a good alternative model. The maps suggest that the halide and potassium occupancies may be nonstoichiometric, but we have not been able to pursue this. Calculations were done with programs of the CRYM X-ray computing system plus ORTEP;[35] scattering factors were taken from the standard compilations.[36] Hydrogen atoms were ignored in the calculations.

Pt_2Br at 19 K. The crystal was cooled to 19 K at a rate of ~2 K/min. During data collection, the temperature was maintained at 19 ± 1 K. After the low-temperature data set was collected, the crystal was slowly warmed in incremental steps to room temperature. At each temperature, the crystal was allowed to equilibrate for 1 h. Then, the unit cell dimensions were determined with the same 15 reflections as used to determine the cell dimensions at 19 K. A plot of the unit cell dimensions as a function of temperature is given in Figure 2. Checks were made for both a doubled unit cell and for an orthorhombic distortion. Scans were taken in reciprocal space along [100], [010], [001], and [110] axes, with the output of the counter circuit connected to a chart recorder. No extra reflections were observed along any axis that would indicate a radical change in cell dimension.[37-39] A full orthorhombic data set was taken and used for refinement in both orthorhombic and tetragonal unit cells. Lattice cell constants and the goodness of fit did not indicate that an orthorhombic distortion had occurred. A partial data set (out to $2\theta = 30°$) assuming a double orthorhombic unit cell found no additional reflections corresponding to the formation of a supercell.

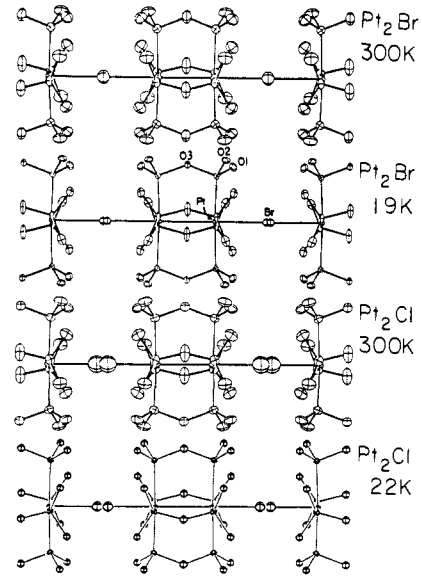

Figure 3. ORTEP drawings of all Pt_2X structures. Ellipsoids are drawn at the 50% probability level.

Table III. Parameters for Pt_2Cl at 300 K

atom	10^4x	10^4y	10^4z	10^4U_{eq}[a]	POP[b]
PtA	0	0	3321 (2)	1.0 (0.3)[c]	2.0
PtB	0	0	3180 (2)	1.1 (0.3)[c]	2.0
Cl	0	0	373 (8)	668 (18)	2.0
K1	2742 (3)	7742	0	402 (5)	4.0
K2	3874 (3)	8874	5000	389 (4)	4.0
P	1174 (1)	1304 (1)	3181 (2)	212 (2)	16.0
O1	2158 (3)	1035 (3)	2189 (6)	340 (8)	16.0
O2	833 (3)	2325 (3)	2570 (6)	363 (9)	16.0
O3	1640 (5)	1492 (5)	5000	437 (14)	8.0
W1	1014 (14)	6014	5342 (21)	3.1 (3)[c]	3.2
W2	410 (54)	5410	2186 (76)	7.9 (14)[c]	1.6
W3	0	5000	586[d]	5.2 (24)[c]	0.4
W4	632[d]	5632	0	4.1 (20)[c]	0.4
W5	4373[d]	9373	1134[d]	3.0 (26)[c]	0.4

[a] $U_{eq} = {}^1/_3(U_{11} + U_{22} + U_{33})$. [b] Atoms per unit cell. [c] B_{iso}. [d] Esd ≥ 100.

The bridging bromide was originally positioned on a center of symmetry between two Pt atoms. However, a large anisotropic thermal parameter describing halide motion along the Pt–Br–Pt bond vector suggested a disordered Br site corresponding to an asymmetric halide bridge. We therefore adopted a model with a disordered, isotropic Br as the bridge. The water molecules W(1) and W(2) were represented by a two-site disorder model similar to that used in the room-temperature structure. A partial drawing of the structure illustrating the 1-dimensional stacking unit is shown in Figure 3; atomic coordinates are given in Table II.

Pt_2Cl at Room Temperature. Preliminary Weissenberg photographs of Pt_2Cl were very similar to those of Pt_2Br and showed no signs of cell doubling. Again, the bridging halide was represented by a two-site model with isotropic thermal parameters. One fully populated water site, W(1), was found, with additional sites of lower partial population in the region near K(1). The structure was refined with both a single platinum atom site and with a two-site model; both gave the same values for the R index and the goodness of fit. Because spectral data indicate that both Pt_2 and Pt_2Cl_2 are present in the crystal, we report the parameters for the model with two platinum sites. A partial drawing of the structure illustrating the 1-dimensional stacking unit is shown in Figure 3; atomic coordinates are listed in Table III.

Pt_2Cl at 22 K. A second crystal of Pt_2Cl was used for the low-temperature studies. After temperature equilibration at 22 K, data collection

(35) (a) Duchamp, D. J. Paper B-17, American Crystallographic Association Meeting, Bozeman, Mt, 1964. (b) Johnson, C. K. *ORTEP, A Fortran Thermal Ellipsoid Plot Program (ORNL-3794)*; Oak Ridge National Laboratory: Oak Ridge, TN, 1965.

(36) *International Table for Crystallography*; Kynoch: Birmingham, England, 1974; Vol. IV, p 72.

(37) Kistenmacher, T. J.; Destro, R.; Marsh, R. E.; Samson, S. *Mol. Cryst. Liq. Cryst.* **1980**, *62*, 173.

(38) Williams, R.; Lowe Ma, C.; Samson, S.; Khanna, S. K.; Somoano, R. B. *J. Chem. Phys.* **1980**, *72*, 3781.

(39) Lowe Ma, C.; Williams, R.; Samson, S. *J. Chem. Phys.* **1981**, *74*, 1966.

Table IV. Parameters for Pt_2Cl at 22 K

atom	10^4x	10^4y	10^4z	10^4U_{eq}[a]	POP[b]
PtA	0	0	3338 (2)	0.22 (3)[c]	2.0
PtB	0	0	3162 (1)	0.22 (3)[c]	2.0
Cl	0	0	316 (9)	287 (10)	2.0
K1	2772 (2)	7772	0	150 (3)	4.0
K2	3892 (2)	8892	5000	134 (3)	4.0
P	1173 (1)	1325 (1)	3174 (1)	90 (2)	16.0
O1	2161 (2)	1073 (2)	2140 (4)	122 (6)	16.0
O2	807 (2)	2353 (2)	2572 (4)	129 (7)	16.0
O3	1659 (4)	1510 (3)	5000	156 (10)	8.0
W1	1030 (10)	6030	5000	1.5 (2)[c]	3.0
W2	0	5000	2272 (60)	1.3 (6)[c]	0.6
W3	0	5000	909 (60)	0.8 (7)[c]	0.5
W4	649 (40)	5649	0	1.4 (6)[c]	0.7
W5	612 (30)	5612	2835 (41)	1.1 (5)[c]	1.2

[a] $U_{eq} = {}^1/_3(U_{11} + U_{22} + U_{33})$. [b] Atoms per unit cell. [c] B_{iso}.

was begun. When a search procedure similar to that done for Pt_2Br was used, no extra reflections were found at low temperature, thus confirming the choice of cell dimensions. An orthorhombic data set was collected as described above for Pt_2Br at 19 K; 3335 reflections were scanned in the range $5° < 2\theta < 80°$. Systematic absences in the diffractometer data of $h01$, where $h = 2n + 1$, and $0k1$, where $k = 2n + 1$, were consistent with space group $P4/mbm$ (No. 127). The data were merged to give 1428 independent reflections, all of which were used in the structure solution and refinement.

Initially, refinement proceeded with ordered platinum atoms but two-site disordered bridging chloride ions. Because this yielded highly anisotropic platinum thermal parameters ($U_{11} = U_{22} = 0.0029$ (1), $U_{33} = 0.0082$ (1)), an alternative model was refined, with the platinum atom also disordered between two sites. Allowing the two half-populated platinum atoms to move along the stacking axis gave a Pt–Pt site separation of 0.142 (2) Å[30] or Pt–Pt bond distances of 2.685 (2), 2.827 (2), or 2.969 (2) Å, depending, as will be discussed later, on the overall translational symmetry. The final R value and goodness of fit were essentially the same as in the ordered model. A partial drawing of the structure illustrating the 1-dimensional stacking unit is shown in Figure 3; atomic coordinates are given in Table IV.

Pt_2I Powder Diffraction. Powder diffraction spectra obtained on a Guinier camera with nickel-filtered Cu Kα radiation indicated an orthorhombic cell for Pt_2I, not a tetragonal cell as observed for Pt_2Cl and Pt_2Br. The unit cell dimensions are $a = 12.67$ (5), $b = 13.52$ (5), and $c = 17.45$ (5) Å. Weissenberg photographs of Pt_2I showed that all crystals studied were twinned. No single-crystal diffraction studies were attempted.

Results

Given the 300 K structure of Pt_2Br reported earlier, our efforts were first directed toward establishing the basic properties and structural variations that occur in Pt_2Br and related systems. We will first discuss the evidence for semiconductor behavior and then address the translational symmetries of the 1-dimensional Pt_2X materials.

Semiconductor Properties of Pt_2Br. Our experiments were limited both by the small crystal size and by the decomposition of the sample. Pt_2Br disproportionates and hydrolyzes in aqueous solution and, on the basis of UV–vis spectra, appears to change slightly during the course of pellet making.

The electrical conductivity of Pt_2Br powder was measured by a contactless microwave technique; the conductivity in the range 100–300 K is shown in Figure 4. The temperature dependence from 100 to 200 K yields a semiconductor bandgap of 0.08 eV. This is comparable to that found for $K_2[Pt(CN)_4]Br_{0.3}\cdot 3.2H_2O$, 0.073 eV,[40] and $Pt_2(CH_3CS_2)_4I$, 0.05 eV.[29] However, the conductivity of Pt_2Br at 300 K ($\sigma = 10^{-3}\ \Omega^{-1}\ cm^{-1}$) is much less than that found in $K_2Pt(CN)_4Br_{0.3}\cdot 3.2H_2O$ ($\sigma \sim 10^3\ \Omega^{-1}\ cm^{-1}$).[41-43] Observation of poor electrical conductivity is usually taken as evidence for a hopping-type conduction process.[42]

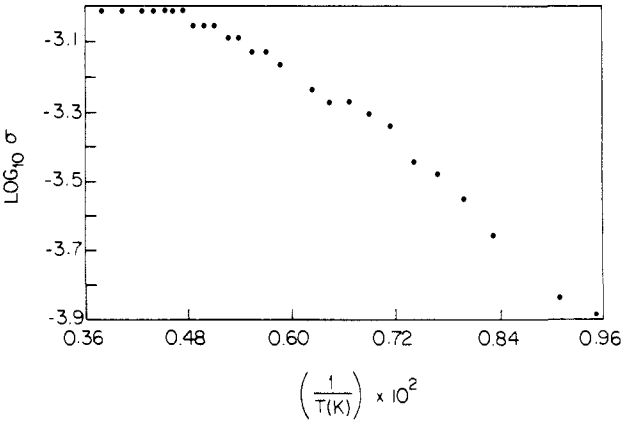

Figure 4. Microwave electrical conductivity of Pt_2Br from 100 to 300 K. Conductivity from 100 to 200 K fitted with an E_a of 0.15 eV for $E_g = E_a/2 = 0.08$ eV.

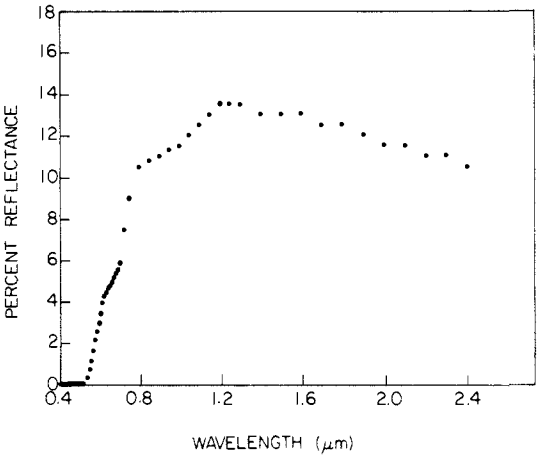

Figure 5. Diffuse reflectance spectrum of Pt_2Br at 300 K.

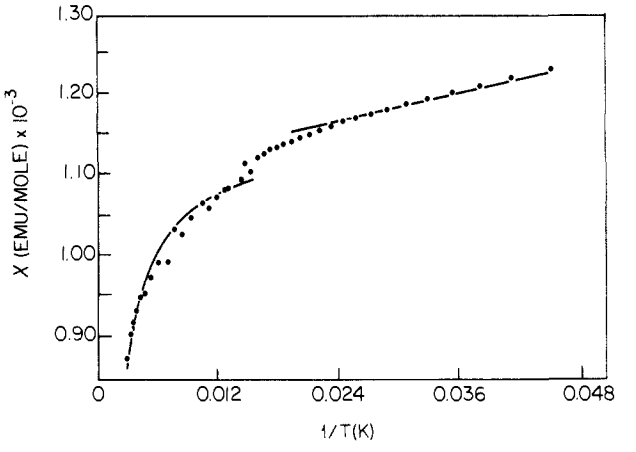

Figure 6. Magnetic susceptibility anomaly of Pt_2Br for the range 22–300 K. From 1.7 to 50 K, the susceptibility data follow Curie–Weiss behavior. For the range 60–300 K, the susceptibility is linearly dependent on temperature.

To seek other evidence of a bandgap, the reflectance spectrum of Pt_2Br at 300 K was measured and is shown in Figure 5. While a plasma edge absorption has been observed for $K_2Pt(CN)_4Br_{0.3}\cdot 3.2H_2O$,[44] no evidence of a similar absorption was seen for Pt_2Br. The strong absorption at 400–600 nm is assigned to intervalence charge transfer.[30]

The magnetic susceptibility was found to be small for all three samples. At low temperatures, all samples obey the Curie–Weiss

(40) Kuse, D.; Zeller, H. R. *Phys. Rev. Lett.* **1971**, *27*, 1060.
(41) Zeller, H. R.; Beck, A. *J. Phys. Chem. Solids* **1974**, *35*, 77.
(42) Miller, J. S.; Epstein, A. *Prog. Inorg. Chem.* **1976**, *20*, 1.
(43) Williams, J. M.; Schultz, A. J.; Underhill, A. E.; Carneiro, K. In *Extended Linear Chain Compounds*; Miller, J. S., Ed.; Plenum: New York, 1982; Vol. 1, Chapter 3.
(44) Geserich, H. P. In *Electronic Properties of Inorganic Quasi-One-Dimensional Compounds*; Monceau, P., Ed.; D. Reidel: Boston, 1985; Vol. 2, p 111.

Table V. Selected Bond Distances (Å) and Angles (deg)

	compound (T, K)				
	Pt_2[a] (300)	Pt_2Br[b] (300)	Pt_2Br[c] (19)	Pt_2Cl[c] (300)	Pt_2Cl[c] (22)
			Bond Distances		
Pt–Pt	2.925 (1)	2.793 (1)	2.781 (1)	2.729 (2)	2.685 (2)
				2.958 (2)	2.969 (2)
Pt–X (short)		2.699 (1)	2.579 (4)	2.281 (7)	2.441 (7)
				2.395 (7)	2.299 (7)
Pt–X (long)			2.778 (4)	2.886 (7)	2.951 (7)
				3.001 (7)	2.809 (7)
ΔX			0.199 (5)	0.606 (9)	0.510 (10)
Pt–P	2.320 (5)	2.334 (1)	2.331 (1)	2.334 (2)	2.335 (2)
				2.331 (2)	2.331 (2)
P—O(H)	1.579 (9)	1.562 (4)	1.572 (4)	1.577 (4)	1.581 (3)
P=O	1.519 (9)	1.505 (4)	1.509 (4)	1.514 (4)	1.518 (3)
P—O (bridging)	1.623 (6)	1.618 (3)	1.621 (6)	1.622 (6)	1.626 (5)
P···P	2.980 (6)	2.935 (2)	2.924 (2)	2.956 (2)	2.949 (1)
O(H)···O	2.505 (19)	2.487 (5)	2.482 (5)	2.476 (6)	2.479 (4)
K(1)···O(H)	2.848 (14)	2.915 (5)	2.861 (8)	2.884 (10)	2.828 (7)
K(1)···O	2.847 (13)	2.912 (6)	2.887 (8)	2.873 (10)	2.850 (7)
			Bond Angles		
Pt–Pt–P	90.67 (10)	91.74 (2)	91.75 (3)	92.78 (6)	93.25 (5)
				89.97 (6)	89.76 (5)
Pt–P–O(H)	114.0 (5)	113.4 (1)	113.1 (1)	114.3 (2)	114.7 (1)
				112.7 (2)	112.7 (1)
Pt—P=O	118.0 (5)	117.3 (2)	117.5 (2)	118.7 (2)	118.4 (1)
				117.7 (2)	117.1 (1)
Pt–P–O (bridge)	110.3 (4)	110.4 (2)	110.4 (2)	109.0 (2)	108.7 (2)
				111.7 (2)	112.1 (2)
P–O–P	133.3 (9)	130.2 (3)	128.9 (4)	131.4 (4)	130.2 (3)

[a] References 24 and 52. [b] Reference 28. [c] This work.

Table VI. Core Shell Binding Energies (eV)

compound	Pt ($4f_{7/2}$)	P (2p)	halide
$K_4[Pt_2(P_2O_5H_2)_4]\cdot 3H_2O$	73.7 (3)	133.6 (3)	
$K_4[Pt_2(P_2O_5H_2)_4Cl]\cdot 3H_2O$	73.8 (2)	133.8 (2)	*a*
$K_4[Pt_2(P_2O_5H_2)_4Br]\cdot 3H_2O$	73.9 (2)	133.6 (3)	69.4 (2)[b]
$K_4[Pt_2(P_2O_5H_2)_4I]\cdot nH_2O$	73.6 (2)	133.4 (2)	619.7 (3)[c]

[a] Not measured. [b] Br ($3d_{5/2}$). [c] I ($3d_{5/2}$).

Table VII. Magnetic Susceptibility

	Pt_2Cl	Pt_2Br		Pt_2I
T, K	1.7–300	1.7–50	60–300	1.7–300
χ_M	$C/(T-\theta)+\chi_{dia}$	$C/(T-\theta)+\chi_{dia}$	$CT+\chi_{dia}$	$C/(T-\theta)+\chi_{dia}$
C	1.76 (7) × 10^{-3}	3.17 (7) × 10^{-3}	−9.7 (4) × 10^{-7}	1.45 (1) × 10^{-3}
θ, K	−0.8 (1)	−1.62 (8)		−0.44 (2)
χ_{dia}	2.21 (3) × 10^{-4}	1.092 (4) × 10^{-3}	1.154 (7) × 10^{-3}	7.52 (6) × 10^{-5}

law with one unpaired spin per ~20 platinum atoms. Both Pt_2Cl and Pt_2I continue to obey the law at room temperature. The Curie–Weiss parameters are given in Table VII.

At higher temperatures, above about 55 K, the Pt_2Br magnetic susceptibility deviates from Curie–Weiss behavior, as shown in Figure 6. The high-temperature susceptibility is distinctly smaller than would be predicted on the basis of the Curie–Weiss parameters derived frm the low-temperature measurements; much of the difference is due to the large χ_{dia} (Table VII). The magnetic susceptibility of Pt_2Br is similar to that observed for $K_2Pt(CN)_4Br_{0.3}\cdot 3.2H_2O$.[45]

Figure 7 shows the results of fitting the high-temperature Pt_2Br magnetic susceptibility to a tight-binding model calculation appropriate for semiconductors.[46] Because of a relatively large correction factor for the sample bucket (at 300 K, only 14% of the volume magnetization is due to the sample), we can only say that the bandwidth is larger than the lower limit of 0.05 eV shown in Figure 7. In summary, Pt_2Br has the magnetic susceptibility properties of a semiconductor at high temperatures (>150 K); the low-temperature magnetic susceptibility is dominated by

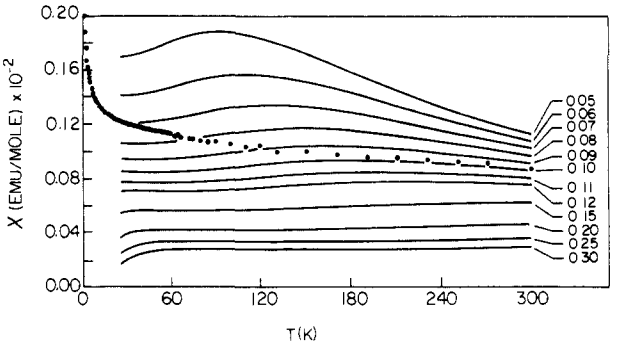

Figure 7. Magnetic susceptibility of Pt_2Br. The solid lines are calculated susceptibilities for a tight-binding model with a range of semiconductor bandwidths.

paramagnetic sites as found for Pt_2Cl and Pt_2I. We do not know whether a transition from semiconductor to insulator occurs at low temperature.

Structural Properties of Pt_2X. The translational symmetries ($(AAB)_n$, $(ABC)_n$, and $(AABCCB)_n$) shown in schemes 1–5 (Figure 1) illustrate different structural arrangements for Pt_2X and imply different patterns of platinum oxidation states; we therefore attempted to assign the oxidation states of the platinum atoms by ESCA. Core-electron binding energies can be studied by ESCA, and oxidation states can often be determined. Evidence for two different oxidation states in other strongly coupled metal systems, either mixed-valence dimers or 1-dimensional conductors, has been presented,[47,48] though the general validity of the results has been questioned on the basis of relaxation effects of the electron hole formed in the ESCA process or asymmetry of the photoionized state.[49] The results of the ESCA study of Pt_2Cl, Pt_2Br, and Pt_2I are listed in Table VI. They provide no conclusive evidence to suggest multiple platinum oxidation states or differing chemical environments for the platinum, bridging bromide or iodide, or ligated phosphorus atoms. It is interesting to note that

(45) Menth, A.; Rice, M. J. *Solid State Commun.* **1972**, *11*, 1025.
(46) Kahn, A. H.; Candela, G. A.; Walatka, V., Jr.; Perlstein, J. H. *J. Chem. Phys.* **1974**, *60*, 2664.
(47) Lazarus, M. S.; Sham, T. K. *J. Am. Chem. Soc.* **1979**, *101*, 7622.
(48) Cahen, D.; Lester, J. E. *Chem. Phys. Lett.* **1973**, *18*, 108.
(49) Hush, N. S. *Chem. Phys.* **1975**, *10*, 361.

all of the electrically conductive samples yield Pt binding energies that are identical with that found for the reduced Pt_2 species, rather than ones that follow the general trend of a 1-eV increase in binding energy for every unit increase in platinum oxidation state.[26]

Both Pt_2Cl and Pt_2Br retain a tetragonal unit cell on cooling to 19 K. The Pt_2Br unit cell dimensions contracted as shown in Figure 2; Pt_2Cl showed a similar reduction of the unit cell dimensions. For Pt_2Br, the temperature dependence of the length of the *c* axis was not as great as that of the *a* and *b* axes, nor did inflection points occur at the same temperature. It is most interesting to note that the unit cell did not double in size along any unit cell axis, although this has been seen in other 1-dimensional systems. Also, no evidence for an orthorhombic distortion was found, nor was any tilting of the Pt–Br–Pt unit with respect to the stacking axis observed.

Tables II–V list the final parameters of the models used to describe the three structures. At 19 K, the Pt_2Br structure was fitted by a single-site model for the platinum atoms and a two-site model for the bridging bromide ion. Of the translational symmetries schematically described in Figure 1, the only ones that permit relatively well-defined platinum atom positions and two-site disorder of the bridging halide are schemes 3–5 with $(ABC)_n$, symmetrically modified $(AAB)_n$, and asymmetrically modified $(AAB)_n$ translational symmetries, respectively. The separation between the linear chains of atoms in these structures is large, 9.3 Å, and thus the interchain structural correlation is expected to be weak. A randomly ordered set of chains of schemes 3–5 will have equal numbers of chains pointing to the left and to the right; an average yields the X-ray diffraction results observed for Pt_2Br at 19 K.

The Pt_2Cl structures were refined with a two-site model for the bridging chloride and both one- and two-site models for the platinum atoms. At both room temperature and at 22 K, the chloride ion sites were well-separated and refined smoothly. At room temperature the Pt could be refined in a single site; changing to a two-site model gave nearly identical results. The resulting $(AABCCB)_n$ translational symmetry is in better accord with spectral data, which will be discussed below, and thus we have accepted it. There is a significant difference in the halide separations between the chloride (0.606 (9) Å) and the bromide (0.199 (5) Å) even though the *c*-axis distance is nearly the same. This difference is larger than expected from the difference in radius between Cl and Br (0.15 Å), although similar to that found for Wolfframs' red salts.[50]

When Pt_2Cl was cooled to 22 K, the chloride and platinum positions remain disordered, and the two-site model is retained. This model is not statistically better than a single-site platinum model (the *R* factor and goodness of fit are each improved by only 0.01), but as in the room-temperature case, it has been adopted because of spectroscopic results.

Because of intimate twinning, the structure of Pt_2I was not determined with single-crystal X-ray diffraction. The crystals of Pt_2I have a magnetic susceptibility similar to Pt_2Cl and Pt_2Br and a dark, metallic appearance.

The Raman spectra of Pt_2Cl and Pt_2Br at ca. 25 K are shown in Figure 8; these spectra are similar to those reported by Kurmoo and Clark.[30b] The wavenumbers of the bands observed for Pt_2Cl are significantly different from those reported earlier,[30b] owing to the fact that different excitation wavelengths were used to obtain the Raman spectra. For Pt_2Cl, we employed 514.5-nm excitation, which is close to the IVCT absorption maximum, while Kurmoo and Clark employed 647.1-nm excitation. We note that the Raman spectrum of Pt_2Br also exhibits unusual relative intensity changes with excitation wavelength. The origin of these differences will be discussed in detail later.[31] Kurmoo and Clark concluded that, on the basis of X-ray work at room temperature, both Pt_2Cl and Pt_2Br consist of polar dimers (scheme 3 with $(ABC)_n$ translational symmetry) and were assigned the band observed at

(50) Clark, R. J. H. In *Advances in Infrared and Raman Spectroscopy*; Clark, R. J. H., Hester, R. E., Eds.; Wiley: Chichester, 1984; Vol. 11, Chapter 3.

Table VIII. Raman Bands (cm^{-1}) for Pt_2Cl[a]

assignment	this work[b]	Clark and Kurmoo[c]
$\nu_1(Pt^{II}–Pt^{II})$	119 (mw)	125.8 (mw)
$\nu_2(Pt^{III}–Pt^{III})$	155 (vs)	152.3 (vs)
ν_3	260 (mw)	263 (mw)
$\nu_3(Pt^{III}–Cl)$	301 (vs)	291.3 (vs)
$\nu_1 + \nu_3$	419 (mw)	418 (w)
$\nu_2 + \nu_3$	453 (m)	443 (ms)
$\nu_3' + \nu_3$	557 (mw)	552 (w)
$2\nu_3$	598 (m)	583 (ms)

[a] Abbreviations: m = medium, v = very, w = weak, s = sharp. [b] λ_0 = 514.5 nm, 25 K, single crystal. [c] Reference 30, λ_0 = 647.1 nm, 80 K, K[ClO_4] disk matrix.

Table IX. Raman Bands (cm^{-1}) for Pt_2Br[a]

assignment	this work[b]	Clark and Kurmoo[c]
δ(Pt–Pt–Br)	93 (w)	93 (w)
ν_1(Pt–Pt)	116.5 (vs)	117 (vs)
ν_2(Pt–Pt)	122 (vs)	122 (vs)
ν_2'(Pt–Pt)[d]	132 (mw)	137 (mw)
?	193 (mw)	195 (mw)
ν_3(Pt–Br)	211 (m)	210 (m)
ν_3'(Pt–Br)[d]	223 (w)	223 (w)
$2\nu_1$	231 (sh)	
$\nu_1 + \nu_2$	236 (m)	
$2\nu_2$	241 (m)	239 (m)
$\nu_2 + \nu_3$	332 (mw)	330 (mw)
$3\nu_2$	260 (mw)	355 (mw)
$2\nu_2 + \nu_3$	454 (w)	450 (w, br)
$4\nu_2$	474 (w, br)	475 (w, br)

[a] Abbreviations: m = medium, v = very, w = weak, s = sharp, sh = shoulder, br = broad. [b] λ_0 = 676.4 nm, 25 K, single crystal. [c] Reference 30, λ_0 = 647.1 nm, 80 K, K[ClO_4] disk matrix. [d] Raman bands attributed to local states; see text.

~152 cm^{-1} in the Pt_2Cl spectrum to the Pt–Pt stretch. The Pt(III)–Pt(III) stretch in the fully oxidized form, Pt_2Cl_2, is observed at 158 cm^{-1}, and the Pt(II)–Pt(II) stretch in the reduced form, Pt_2, is at 115 cm^{-1}. If a polar dimer represents the true structure for Pt_2Cl, we would expect a Pt–Pt stretching mode intermediate in wavenumber to those found for Pt_2 and Pt_2Cl_2. Accordingly, we believe that the ~152-cm^{-1} band (155 cm^{-1} in our spectrum) of Pt_2Cl should be assigned to the Pt(III)–Pt(III) stretch of the oxidized unit in a chain with $(AABCCB)_n$ translational symmetry. The band at 119 cm^{-1} in Pt_2Cl is attributed to the Pt(II)–Pt(II) stretch of the reduced unit in the chain. The fact that the two bands assigned to Pt–Pt stretching in Pt_2Cl are quite close to those observed for the fully oxidized and fully reduced forms suggests strong valence localization for Pt_2Cl. The band at ~301 cm^{-1} in Pt_2Cl is attributed to the symmetric Pt(III)–Cl stretch.

The Raman spectrum of Pt_2Br shows bands at ~117 and ~122 cm^{-1}. While the band at 117 cm^{-1} is quite close to the Pt(II)–Pt(II) stretching frequency of Pt_2, the 122-cm^{-1} feature is significantly lower than the 132-cm^{-1} Pt(III)–Pt(III) stretching frequency of Pt_2Br_2.[30] Furthermore, the Pt–Br stretch of Pt_2Br is 211 cm^{-1}, by contrast to 223 cm^{-1} for Pt_2Br_2. The wavenumbers for the Pt–Br and "Pt(III)–Pt(III)" stretching modes are inconsistent with complete valence localization and $(AABCCB)_n$ translational symmetry. The two Pt–Pt stretches could result from coupling of two Pt–Pt bonds of equal or nearly equal strengths, as would be expected for schemes 3–5. However, the appearance of only one band attributable to a Pt–Br stretching mode suggests that scheme 4, the symmetrically modified $(AAB)_n$ structure, provides the best description. The bands at ~132 and ~223 cm^{-1} are sample dependent in their intensities and wavenumbers (note that Clark and Kurmoo reported a band at 137 cm^{-1}). We attribute these two bands to Pt–Pt and Pt–Br stretches, respectively, of a local state. The presence of local states in these systems will be addressed in a later paper.[31] The observed Raman bands and their assignments are given in Tables VIII and IX.

The relative intensities of the bands attributed to the Pt–Pt and Pt–X stretching modes also provide information concerning the

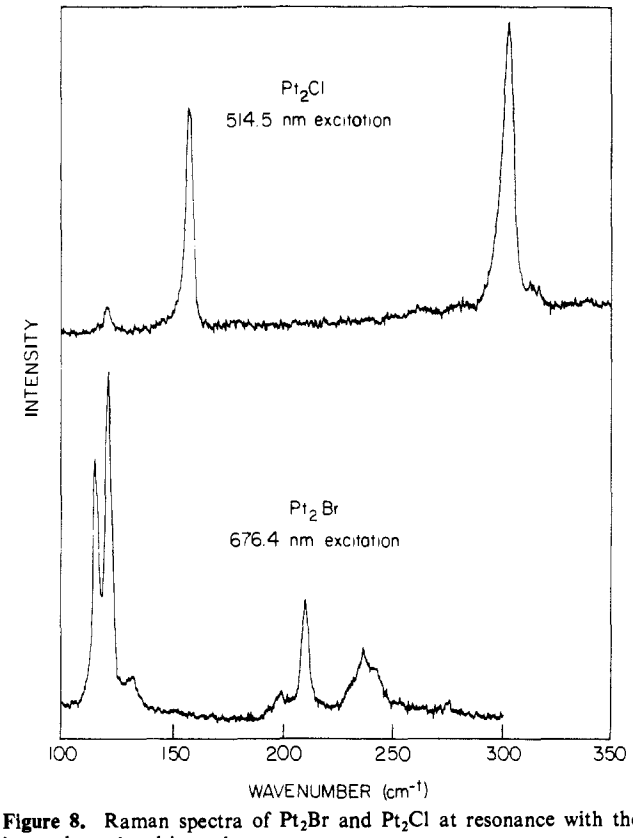

Figure 8. Raman spectra of Pt_2Br and Pt_2Cl at resonance with the intervalence band in each case.

structures of these materials. The ν(Pt–Cl) is intense relative to the ν(Pt–Pt) bands of the Pt_2Cl complex, while ν(Pt–Br) is weak relative to the ν(Pt–Pt) bands of Pt_2Br. These observations are consistent, with a significant shift of the Cl atom from the central position between the dimer units but with the Br atom being quite close to this special position.

The Raman spectra of Pt_2Cl and Pt_2Br do not change significantly on going from 25 K to room temperature, indicating that there is no structural phase transformation over this temperature range. The wavenumbers and widths of the Raman bands do vary slightly with temperature, as is expected. The temperature dependence of the far-IR spectra also shows no evidence for structural phase transformations.

Discussion

A tetragonal unit cell has been found for the parent dimer, $K_4[Pt_2(P_2O_5H_2)_4]\cdot 3H_2O$, Pt_2, and the 1-dimensional materials $K_4[Pt_2(P_2O_5H_2)_4Cl]\cdot 3H_2O$, Pt_2Cl, and $K_4[Pt_2(P_2O_5H_2)_4Br]\cdot 3H_2O$, Pt_2Br. The c axis length is very similar for Pt_2Cl and Pt_2Br systems and only slightly reduced for Pt_2. We conclude that the $Pt_2(P_2O_5H_2)_4$ cores and the K^+ ions form a stable arrangement. We note the disorder found in the water positions and the fact that no disorder was evident in the K^+ ion positions. Replacement of K^+ by Na^+ causes a major structural change in Pt_2 (from tetragonal to an orthorhombic unit cell);[26] we conclude that the alkali-metal ion has an important structural influence. The Pt_2I structure differs from that found for Pt_2Cl and Pt_2Br.

This regular array of potassium ions and Pt–Pt units fixes the coordination environment for bridging chloride or bromide (with potassium as the counterion) as a tetragonal cavity approximately 5.34 Å long. This distance corresponds to the Pt–Pt distance between neighboring dimers along the stacking axis. From the structures of fully oxidized Pt_2X_2 complexes, one finds the following Pt–X bond distances: Pt–Cl = 2.407 (2), Pt–Br = 2.572 (1), and Pt–I = 2.742 (1) Å.[28,30,51] Thus, a chloride ion is not constrained along the c axis, a bromide ion just fits, and an iodide ion is too large for the cavity (which may explain why the iodide complex does not crystallize in the same space group).

The crystallographic data for Pt_2Br are consistent with a regular array of Pt–Pt–Br units, as described by schemes 3–5. However, on the basis of the Raman data, namely the fact that the polar dimer of $(ABC)_n$ translational symmetry and the asymmetrically modified $(AAB)_n$ translational symmetry should yield spectra in which there are two bands attributable to Pt–Br stretches, schemes 3 and 5 can be ruled out, since only one such band is observed for Pt_2Br. Thus, scheme 4, the "intermediate" between the extremes of $(AAB)_n$ and $(AABCCB)_n$, best describes the Pt_2Br structure. Scheme 4, with the symmetrically modified $(AAB)_n$ translational symmetry, requires both a short and a long Pt–Br bond; at 19 K, bond distances of 2.579 (4) and 2.778 (4) Å were found. At least in the limit of a short chain, we would not expect a large energy barrier for halide "atom transfer",[52] as shown below:

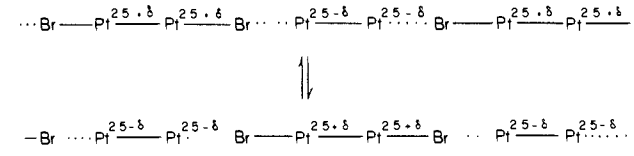

Consequently, halide motion should be thermally activated and, at 300 K, would be rapid. The 300 K X-ray structural results are consistent with fast halide motion in either an upper vibrational state or a centrally positioned bromide. We recall, however, that the room-temperature Raman spectrum shows evidence for a band attributable to a Pt–Br stretch, demonstrating that the bromide ion remains slightly shifted, even at room temperature, from the special position equidistant from neighboring Pt atoms. Scheme 4 also allows for a very slight variation in Pt–Pt bond length, such that it may or may not (depending upon the sensitivity of the technique and the value of δ) be possible to resolve two distinct Pt–Pt bonds. Raman data do, in fact, give evidence for two bands attributable to Pt–Pt stretches, these being very close in wavenumber (ca. 116.5 and 122 cm^{-1}), whereas the X-ray data do not require two distinct Pt–Pt bond lengths. Comparison of the isotropic thermal ellipsoids for the Pt atoms in Pt_2Br at 19 K (Table II) and in Pt_2Cl at 22 K (Table IV) shows that the Pt atom thermal motion in Pt_2Br (0.074 Å) is larger than that in Pt_2Cl (0.053 Å). Thus there may, in fact, be two distinct Pt–Pt bonds in the Pt_2Br structure. The Pt–Pt distance of 2.781 (1) Å at 19 K, which reflects a formal Pt–Pt bond order of 0.5, is intermediate between those observed for the reduced dimer Pt_2, d(Pt–Pt) = 2.925 (1) Å,[24,53] and the fully oxidized Pt_2Br_2, d(Pt–Pt) = 2.716 (1) Å.[30c,51]

The translational symmetry of the Pt_2Cl structure is different from that of Pt_2Br and appears at both room temperature and 22 K to be a combination of equal amounts of Pt_2 and Pt_2Cl_2 alternating along the chains. The spectral and magnetic susceptibility data suggest that the symmetry is $(AABCCB)_n$ at both temperatures. The magnetic susceptibility data do not show any structural transition between high and low temperature; this result is expected if $(AABCCB)_n$ is the exclusive structural component.

Whangbo and Canadell have performed band calculations using extended Hückel methods and halide p-orbitals and metal d-orbitals on a model for the Pt_2X systems, $Pt_2(HCS_2)_4I$.[12] They have discussed the results both in terms of a possible Peierls instability of a metallic system and in terms of localized electronic states of a nonmetallic system. In neither limit did the $(ABC)_n$ translational symmetry represent an energy minimum; instead, $(AABCCB)_n$ was predicted to be more stable than $(AAB)_n$ by 4 kJ mol^{-1}. The slight discrepancy between the interpretation of our experimental results for Pt_2Br and this calculation is interesting, particularly in light of past success of calculations in the analysis of $K_2[Pt(CN)_4]Br_{0.3}\cdot 3.2H_2O$.[9] The results show that the subtle balance of forces (i.e., electron–phonon coupling, etc.) in

(51) Alexander, K. A.; Bryan, S. A.; Fronczek, F. R.; Fultz, W. C.; Reingold, A. L.; Roundhill, D. M.; Stein, P.; Watkins, S. F. *Inorg. Chem.* **1985**, *24*, 2803.

(52) Burdett, J. K. *Inorg. Chem.* **1978**, *17*, 2537.

(53) Marsh, R. E.; Herbstein, F. H. *Acta Crystallogr., Sect. B: Struct. Sci.* **1983**, *B39*, 280.

the Pt_2X systems gives rise to different ground-state structures for Pt_2Cl and Pt_2Br.

Pt_2Br is a moderate semiconductor, with conductivity 10^6 times greater than that of Reihlen's green, $[Pt^{II}(etn)_4][Pt^{IV}(etn)_4Br_2]Br_4 \cdot 4H_2O$ (etn = ethylamine),[50] but 10^6 times weaker than that of $K_2[Pt(CN)_4]Br_{0.3} \cdot 3.2H_2O$. The conductivity shows an unusual temperature dependence and, most likely, it also shows sample dependence, given the sample dependence observed in the Raman data and in the visual appearance. The present conductivity results are consistent with a thermally activated electrical conductivity process also referred to as a hopping process.[42] The actual mechanism may be related to the intrinsic structure as well as to the local states (polarons, bipolarons, kinks) that can arise from chemical defects. Recent resonance Raman studies of $[Pt(en)_2][Pt(en)_2X_2](ClO_4)_4$, where X = Cl or Br, have shown evidence for fine structure in the ν_1(Pt-Br) band, demonstrating the presence of more than one structural species. Conradson et al.[54] attribute this fine structure, in part, to the presence of local states that arise from chemical defects. Baeriswyl and Bishop[55] have recently developed a theory of charge-transfer instability in quasi-1-dimensional mixed-valence metal systems and have calculated optical properties for local states in these solids.

We note that an analogous system that uses iodide ion as the bridging unit between metal dimers, $Pt_2(CH_3CS_2)_4I$, forms a structure at 300 K with translational symmetry that is virtually $(AAB)_n$.[29,30] The conductivity of this material is comparable to those of the Pt_2X systems described here.

Conclusion

This paper presents a study of the translational symmetry properties of a unique class of 1-dimensional materials based on a metal dimer as the synthetic unit. The parent metal dimer complex, $[Pt_2(P_2O_5H_2)_4]^{4-}$, with K^+ as the counterion, provides the basic structural framework.

The translational symmetry, $(AAB)_n$, which we anticipated for Pt_2Br, was not found in any structure, although the observed structure is only slightly different from this translational symmetry. Consideration of the cavity size between Pt_2 units indicates that bromide is more appropriate than chloride for creating a highly symmetric 1-dimensional material with $(AAB)_n$ symmetry. Chloride, which is not as well suited for the K^+/Pt_2 framework as bromide, leads to the $(AABCCB)_n$ structure. The Pt_2Cl and Pt_2Br complexes provide an interesting example of how competing interactions in a quasi 1-dimensional system lead to different ground-state structures. An understanding of the relationship between the structures of these materials, the nature of the local states, and the macroscopic properties such as conductivity is essential in developing materials with useful properties.

Acknowledgment. We thank Dr. Sten Samson for many enlightening discussions regarding structural transformations and Dr. Richard E. Marsh for help in interpreting the X-ray results. This research was supported by National Science Foundation Grants CHE84-19828 (H.B.G.) and CHE82-19039 (X-ray diffraction equipment), the Exxon Educational Foundation (W.P.S.), and the LANL Center for Material Sciences (B.I.S.).

Registry No. $K_4[Pt_2(P_2O_5H_2)_4Cl] \cdot 3H_2O$, 99632-89-0; $K_4[Pt_2(P_2O_5H_2)_4Br] \cdot 3H_2O$, 85553-24-8; $K_4[Pt_2(P_2O_5H_2)_4I]$, 85553-25-9; Pt, 7440-06-4.

Supplementary Material Available: Tables of anisotropic thermal parameters (3 pages); listings of observed and calculated structure factors (27 pages). Ordering information is given on any current masthead page.

(54) Conradson, S. D.; Dallinger, R. F.; Swanson, B. I.; Clark, R. J. H.; Croud, V. B. *Chem. Phys. Lett.* **1987**, *135*, 463.
(55) Baeriswyl, D.; Bishop, A., to be submitted for publication.

Kinetics, Mechanism, and Thermodynamic Aspects of the Interconversion of Complexes of Planar and Nonplanar Metallo-Amido-*N* Groups

Terrence J. Collins*[1a] and John T. Keech[1b]

Contribution No. 7453 from The Chemical Laboratories, California Institute of Technology, Pasadena, California 91125. *Received December 23, 1986*

Abstract: The isomerization kinetics of *trans*- (**1**) and *cis*-α-Os(η^4-CHBA-DCB)$(OPPh_3)_2$ (**2**) (H_4CHBA-DCB = 1,2-bis(3,5-dichloro-2-hydroxybenzamido)-4,5-dichlorobenzene) have been studied for the processes $\mathbf{2} \rightarrow \mathbf{1}$ and $\mathbf{2}^+ \rightleftharpoons \mathbf{1}^+$. The trans isomer contains planar amido-*N* ligands and the cis-α isomer contains nonplanar amido-*N* ligands. Each isomerization is first order in metal complex and zero order in $OPPh_3$. The following mechanisms have been considered: D_L, dissociation of a monodentate ligand followed by isomerization and recoordination; D_{C^-}, dissociation of a phenolate anion followed by isomerization and recoordination; $D_{C\cdot}$, dissociation of a phenoxide radical followed by isomerization and recoordination; T, an intramolecular twist mechanism. In both systems the accumulated evidence is most consistent with T mechanisms. The forward rate constants for the $\mathbf{2} \rightarrow \mathbf{1}$ isomerization and the composite rate constants for the $\mathbf{2}^+ \rightleftharpoons \mathbf{1}^+$ equilibrium show minimal sensitivity to solvent polarity and added *p*-toluenesulfonic acid. Isomerizations conducted in the presence of OP(*p*-tolyl)$_3$ show no evidence of incorporation of OP(*p*-tolyl)$_3$ in the final product. When the $\mathbf{2} \rightarrow \mathbf{1}$ isomerization is conducted in neat 2-mercaptoethanol or in the presence of excess hydroquinone, no evidence of radical intermediates is observed. Variable-temperature studies of the equilibrium $\mathbf{2}^+ \rightleftharpoons \mathbf{1}^+$ yielded ΔH° = 12 (3) kcal·mol^{-1} and ΔS° = 42 (2) eu from a van't Hoff plot. Combining these data with the composite rate constants ($k_{obsd} = k_1 + k_{-1}$) allowed separation of the forward (k_1) and reverse (k_{-1}) rate constants. Activation parameters were evaluated from Eyring plots: for $\mathbf{2}^+ \rightarrow \mathbf{1}^+$, $\Delta H^\ddagger$ = 23.7 (6) kcal·mol^{-1} and $\Delta S^\ddagger$ = 17 (2) eu; for $\mathbf{1}^+ \rightarrow \mathbf{2}^+$, $\Delta H^\ddagger$ = 11.5 (6) kcal·mol^{-1} and $\Delta S^\ddagger$ = −25 (2) eu; for $\mathbf{2} \rightarrow \mathbf{1}$, $\Delta H^\ddagger$ = 21.6 (2) kcal·mol^{-1} and $\Delta S^\ddagger$ = 0.3 (6) eu. The activation parameters are discussed.

The organic amide is a central functional group. Planarity of the organic amide is a structural generality having many notable consequences including, together with hydrogen bonding, a controlling function over the secondary structure of proteins. Organic

0002-7863/88/1510-1162$01.50/0 © 1988 American Chemical Society